KINETICS, CATALYSIS, AND REACTION ENGINEERING

Fluid Dynamic Efficiency and Scale-up of a Retreated Blade Impeller CSTR

Marina Campolo, Alessandro Paglianti,† and Alfredo Soldati*

Centro Interdipartimentale di Fluidodinamica e Idraulica and Dipartimento di Scienze e Tecnologie Chimiche, Università di Udine, 33100 Udine, Italy

Numerical simulations are used to characterize the fluid dynamic behavior of an industrial-size reactor. First, we focused on an experimental replica (∼440:1 volume ratio) of the full-scale reactor and evaluated the reliability of fully three-dimensional, time-dependent numerical computations of the flow field. An experiment was planned to obtain power data, which were compared with computer simulations for the scaled model, giving good agreement. Next, we examined the full-scale industrial reactor by exploiting the available macroscopic experimental observations and original computer simulations. We verified the scale-up of the two reactors by comparing the power number, discharge flow number, and pumping efficiency. Finally, by examining the power and stirring capability for different operating conditions, we found the operating conditions that ensured the optimum fluid dynamic efficiency.

1. Introduction

The scale-up of industrial devices from laboratory to plant size is a crucial issue in the design of industrial processes. Tuning of the operating parameters is often necessary for the plant installation to be run under the appropriate conditions or even under suboptimal conditions. However, the additional costs due to such tuning can modify the economics of the plant. When present, continuously stirred-tank reactors (CSTRs) are critical devices in the tuning phase of process parameters, since they represent a large fraction of the overall cost of plant operation. In industrial practice, laboratory experiments are usually planned ahead of the design of the industrial application, yet correlations available for scale-up are not always sufficient to ensure optimal operating conditions. In particular, the CSTR process parameter that changes most when scaled is the mixing time.[1] An incorrect scale-up often determines values larger than optimal for this parameter, thus increasing power consumption. Accurate optimization of process parameters at the final industrial scale is thus required to circumvent this problem.

Extensive experimental industrial-scale investigations are seldom available because of the obvious costs and difficulties in performing research on full-scale plants. Even though laboratory-scale experiments[2,3] can be carried out fairly easily and the influence of tank geometry and process parameters can be examined at low cost,[4,5] no correlation is yet available to scale laboratory-size mixing up to industrial-size installations.[6] An alternative to costly and complex large-scale experiments is to solve the balance equations numerically, thus yielding detailed information on the fluid dynamics and mixing processes.

In this work, we try to identify the optimal fluid dynamic conditions for operating an industrial-size CSTR equipped with two beaver-tail baffles and a retreated curved-blade impeller. This reactor type is widely used for chemical and pharmaceutical production and is glass-lined. We use numerical simulations to calculate the fully three-dimensional time-dependent flow field in the tank as a careful description of the flow field is fundamental to optimization of the mixing time. We focus first on a laboratory-scale replica of the industrial-size reactor (volume ratio of ∼440:1) and compare experimental measurements made for this reactor with results from numerical simulations. In particular, we compare power consumption, which is a macroscopic datum strictly dependent on the fluid dynamics of the reactor. Second, we perform flow-field simulations for the industrial-size reactor. We calculate the power consumption, the discharge flow, and the pumping efficiency for different operating conditions. We verify that numerical simulations done for the industrial reactor and for the laboratory reactor can be represented by approximately the same scale-up curves using dimensionless parameters, i.e., fluid dynamics at the industrial scale can be validated by data collected at the laboratory scale. Finally, we use experimental data available for the industrial installation for further validation of the computed flow fields. We use the detailed flow calculations to identify the operating conditions that result in optimal fluid dynamic efficiency, i.e., the conditions under which the ratio between the flow discharged by the impeller and the power required to operate the impeller is a maximum. In a further development of this work, the calculated flow field will be used to evaluate and optimize the mixing process.[30]

* Corresponding author. E-mail: soldati@uniud.it. Phone: 0432-558864. Fax: 0432-558803. Web: http://158.110.50.22.

† Dipartimento di Ingegneria Chimica, Università di Pisa, 56100 Pisa, Italy.

10.1021/ie010225y CCC: $22.00
Published on Web 12/20/2001

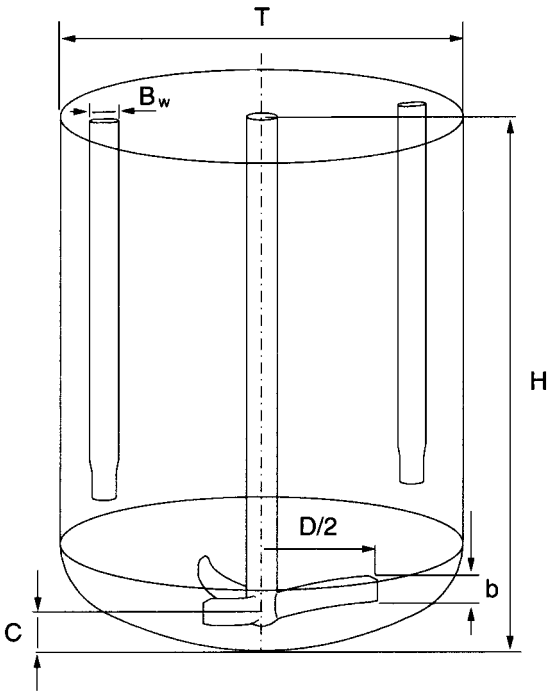

Figure 1. CSTR configuration for experimental and computational analysis. Three-blade, retreated curved-blade impeller is very near the curved bottom. Two beaver-tail baffles are used to increase axial circulation. Geometrical dimensions are reported in Table 1.

2. Methodology

2.1. Experiments. An experimental activity was planned to measure power consumption. We chose this parameter for validation of the computational simulations because (i) power consumption is strictly related to, and representative of, the complex three-dimensional turbulent flow field developing in the vessel; (ii) power consumption is the significant industrial datum; and (iii) measurements of power consumption are simple and reliable. The experimental setup is shown in Figure 1. It comprises an open glass vessel with a torospherical bottom that is equipped with a retreated curved-blade impeller powered by a 2-kW variable-speed motor (maximum angular velocity of 1100 rpm). The impeller is in the curved part of the tank near the bottom, and two beaver-tail baffles are placed at an angle 165° of near the wall of the tank to improve flow circulation and stirring. The dimensions of the vessel and impeller are given in Table 1, and for the sake of comparison, the dimensions of the industrial-size reactor are also listed in Table 1, as the reactor is a laboratory-scale replica of the industrial-size reactor under investigation. The shaft of the impeller is coupled to an instrumented shaft equipped with two strain gauges (xy21-3/120, Hottinger Baldwin Messtechnik) and a digital tachometer (accuracy of ±1 rpm). The strain gauges are wired to a slip-ring assembly (Michigan Scientific Corporation), which is connected to a signal conditioner and amplifier system (MVD 2555, Hottinger Baldwin Messtechnik). A data-acquisition system board (PCI-MIO-16E-4, National Instruments) connected to a computer is used to record and analyze all signals.

To measure power consumption, we recorded continuously both the angular velocity and the torque at the shaft. We measured the data with a sampling frequency of 0.1 kHz and recorded 10 000 points for each acquisition. Each experimental point is averaged over six acquisitions.

Table 1. Geometric Dimensions of Vessel and Impeller for Experimental Setup and Industrial Installation and Values of Dimensionless Parameters[a]

		experimental setup	industrial installation
tank diameter	T	0.308 m	2.348 m
liquid height	H	0.400 m	3.15 m
liquid volume	V	28.29 L	12 500 L
baffle width	B_w	0.025 m	0.170 m
number of baffles	n_B	2	2
impeller diameter	D	0.180 m	1.35 m
impeller clearance	C	0.015 m	0.109 m
blade width	b	0.021 m	0.170 m
number of blades	n_b	3	3
dimensionless parameters[b]	D/T	0.584	0.576
	H/T	1.33	1.33
	B_w/T	0.081	0.073
	b_{eq}/T	0.102	0.108

[a] Scale factors from laboratory to industrial size are 1:7.6 for linear dimensions and ∼1:440 for volumes. [b] Dimensionless parameters are used for evaluation of empirical power characteristic curves for laboratory and industrial vessels. The geometrical similarity is almost perfect.

To ensure the repeatabiliy of the measurements, the system was calibrated periodically by disconnecting the shaft, placing it horizontally on supports, and measuring the strain gauge signal under a specified torque. We observed a linear relation between torque and signal in the working range, and no significant change occurred over time.

Customarily, the operating conditions and power consumption are represented by the corresponding dimensionless groups Reynolds number, *Re*, and power number (or Newton number), *Ne*, defined as

$$Re = \frac{\rho N D^2}{\mu}, \quad Ne = \frac{P}{\rho N^3 D^5} \tag{1}$$

where ρ and μ are the liquid density and viscosity, respectively; N is the angular velocity (rpm); D is the impeller diameter; and P is the power. To vary the Reynolds number in the experiments, the angular velocity of the impeller was varied in the range 80−200 rpm, and the viscosity of the working fluid was varied in the range (1.0×10^{-3})−(825.0×10^{-3}) Pa·s by mixing water and glycerol appropriately. This ensured that the torque was measured in a range carefully chosen to minimize error. This error, however small, requires careful evaluation for an adequate benchmark for the computer simulations to be obtained. Considering that, in the fully turbulent regime, i.e., $Re > 10^4$, the power number is independent of *Re*,[1,7,8] we found that the average experimental value of *Ne* in the turbulent range was 0.697, characterized by an average error of 6% and a maximum error of 16%. The results of the experimental work are shown in Figure 4.

2.2. Simulations. To calculate the three-dimensional, time-dependent flow field inside the CSTR, the volume of the reactor was discretized into finite volumes, as shown in Figure 2. A tuning procedure and grid-independence analysis[9,10] led to the computational domain shown in Figure 2. The cylindrical body of the tank is $27 \times 36 \div 144 \times 45$ in $r \times \theta \times z$ directions, and the curved bottom containing the impeller is $27 \times 36 \div 144 \times 30$. Precisely 136 592 finite volumes were used to shape the impeller and the tank, with care being

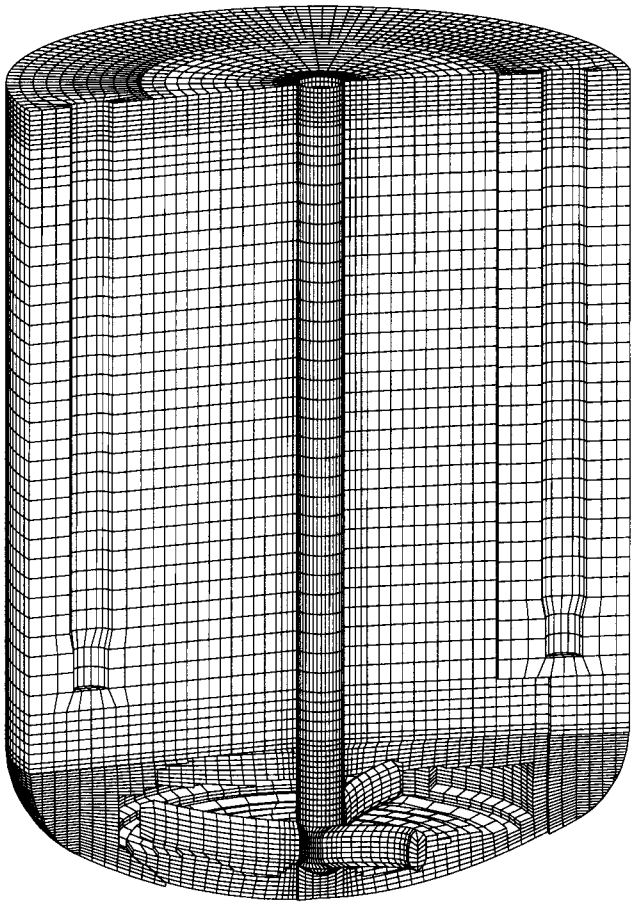

Figure 2. Computational domain used to model both laboratory and industrial vessels. The curved bottom and impeller inside belong to the rotating region. Rotation is counterclockwise. The grid resolution is finer for the impeller region, baffles, and wall layer.

taken to refine the mesh in the impeller and baffle regions, where the velocity spatial gradients are expected to be large. We solved the balance equations for the fluid using a transient, sliding-mesh approach to best simulate the effects of the impeller rotation. This approach has been successfully applied to standard vessels stirred by Rushton,[11] axial,[9] and pitched-blade impellers[12] and to nonstandard, curved-bottom vessel.[13] The fully transient, sliding-mesh approach merits some explanation. Because the position of the baffles relative to the impeller changes continuously while the impeller rotates, the flow field in the tank changes continuously through time. A detailed flow-field simulation requires calculation of the flow field at each incremental position of the impeller. The sliding-mesh approach uses two computational subgrids: (i) one around the impeller (rotating region) comprising 46 152 cells and (ii) one for the rest of the vessel (static region) comprising 90 440 cells. A rotating frame and a fixed frame of reference are used to solve the fluid equations in regions i and ii, respectively. The boundary conditions set on the surface of the cells adjacent to the two regions were updated at each incremental time step. For each examined angular velocity, we ran trial simulations aimed at verifying the influence of the time step on the accuracy and convergence rate. For each simulation, we found the optimal time step to be equal to $^1/_{120}$ of the impeller revolution period.[11] The computation started from the initial condition of fluid at rest in the entire domain, and the flow field was allowed to evolve as driven by the impeller until a pseudo-steady state was attained. This method appears to be the natural method of simulating the flow field in a CSTR, and yet, because of its computational requirements, including long transients, highly refined grids, and robust computational techniques, we are not aware of many examples in the literature.[9,11−13] Rather, recent works make use of steady-state approaches,[14,15] which, however, supply only the time-averaged solution of the flow field.

In the CSTR under consideration, we were interested in examining the operating conditions corresponding to a turbulent flow field. We therefore solved the fluid balance equations in the Reynolds-averaged form, employing a standard $k-\epsilon$ model to reproduce the effects of turbulent fluctuations. The $k-\epsilon$ model is complemented by the algebraic "law of the wall" to reproduce the turbulent flow up to the near-wall regions. The $k-\epsilon$ model is among the simplest turbulence models, as turbulence effects are modeled by the solution of the two scalar equations for kinetic energy transport and dissipation rate. The use of this simplified turbulence model ensures accurate results, comparable to those obtained with more complex turbulence models (renormalization group $k-\epsilon$ models, large eddy simulation models, etc.) provided that the grid is sufficiently refined near the boundaries.[16,17] Despite the anisotropic behavior of turbulence in a baffled agitated vessel, the $k-\epsilon$ model is able to predict the mean instantaneous and time-average features of the flow pattern.[18,19]

In all experiments, the fluid in the tank is bounded by an upper atmosphere. Three-dimensional, time-dependent waves are bound to form at the interface, and sophisticated, computationally demanding algorithms are required to reproduce their dynamics.[13,20] In the present work, which required extensive simulations for a number of different operating conditions, we decided to consider a flat upper free surface, i.e., free shear boundary conditions, to limit the computation effort required.

We performed simulations for (a) the laboratory vessel and (b) the industrial-size reactor. The geometry used in the two cases is the same, except for small details.[21]

3. Results

In this section, we compare our computer simulations with the experiments for the laboratory reactor and a well-known semiempirical power-characteristic curve. This curve was calculated by Nagata[7] using extensive experimental investigations and theoretical modeling and is customarily used to size CSTRs as (i) it can be adapted to a number of different geometries and operating conditions and (ii) it often represents the only reference for evaluating power consumption in some industrial configurations until experiments become available. We report the algebraic details of this curve for our geometry and operating conditions in the Appendix. We use this curve as a reference for the qualitative evaluation of our results.

The industrial-size reactor is the top-line product of a well-known industrial company (Tycon-Technoglass). The producers were able to probe the power consumption for one specific set of operating conditions. We used this measurement to discuss the accuracy of our computer simulations and the reliability of the Nagata curve.[7]

3.1. Convergence to Pseudo-Steady State. Experimental measurements and correlations[7] are reported relative to the pseudo-steady state of the reactor. Once the impeller is set in motion at a constant angular velocity from conditions of still fluid, after a few impeller revolutions, the flow field becomes pseudo-steady in that its time-dependence is limited to the impeller frequency. Thus, if we neglect the so-called macro-instabilities,[22,23] the value of any flow variable averaged over one period is the same regardless of the period chosen. The pseudo-steady state is achieved after a few minutes under the experimental conditions. However, because, for the grid used, the calculation of the flow field for one impeller revolution takes about 18 000 s of CPU time on a 2 × 400-MHz processor with a 1-Gb RAM server, and because on the order of 30−40 revolutions is required to reach the pseudo-steady state, we carefully monitored representative flow variables to ensure that the flow field was steady. We decided to follow over time, i.e., for an increasing number of impeller revolutions, the behaviors of the upward flow rate, the component of momentum in the azimuthal direction, and the power. The time behaviors of these variables are shown in Figure 3 for the laboratory-scale reactor for the operating conditions corresponding to test L4 of Table 2.

We define the upward flow rate, or upflow w_{up}, as the integral across a section normal to the rotation axis of upward-directed fluxes

$$w_{up} = \int_{A^+} \rho \mathbf{v} \cdot d\mathbf{A}_z = \int_{A^+} \rho v_z \, dA_z, \quad \text{where } A^+ = \{d\mathbf{A}_z \in \mathbf{A}_z | \mathbf{v} \cdot d\mathbf{A}_z > 0\} \quad (2)$$

where $\mathbf{v}$ is the velocity, ρ is the density, $\mathbf{A}_z$ is the section normal to the rotation axis, and A^+ is the portion of the section normal to the rotation axis where the axial component of velocity, v_z, is directed upward. This variable can be used to measure the stirring capability of the reactor in the vertical direction (secondary circulation flow). The evolution in time of the upflow profile is shown in Figure 3a. At each time, the upflow profile is obtained by calculating the sum of the upward fluxes over sections at different distances from the impeller. At first, most of the fluid is at rest, and only the fluid close to the impeller blades moves. As the flow develops, reaching the wall of the tank and the baffle, the fluid streamlines are deflected upward, and the upper regions are progressively driven into motion. After 20 impeller revolutions, the upflow profile becomes steady. Because averaging one variable over the horizontal plane corresponds to averaging over one rotation period, the steady profile indicates that the pseudo-steady state is achieved. Yet, the steadiness of the upflow profile is a first but not ultimate measure of convergence to a fully developed flow field.

The azimuthal component of the momentum, M_θ, is defined as the volume integral of the azimuthal velocity, v_θ

$$M_\theta = \int_V \rho v_\theta \, dV \quad (3)$$

where V is the volume of fluid. Variations in M_θ account for modifications of the azimuthal structure of the flow and can be related to the stirring capability of the reactor in the azimuthal direction (primary flow). The behavior of the azimuthal momentum is shown in Figure 3b. When the impeller is set into motion, the fluid between the blades follows, and the azimuthal component of momentum increases quickly during the first revolutions. In the region far from the impeller (near the free surface), the fluid acquires azimuthal momentum only after the upward motion has reached the upper layers of the tank.

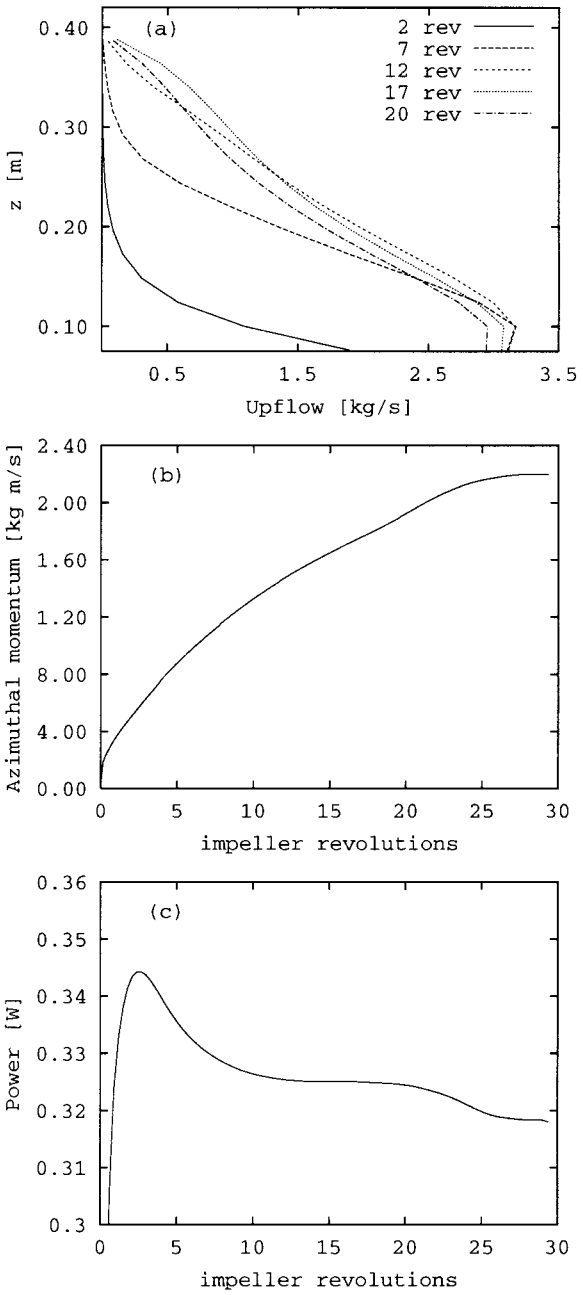

Figure 3. Evolution of gross flow characteristics used to assess convergence to pseudo-steady state: (a) upflow profile, (b) azimuthal component of momentum, and (c) power input. Values are calculated for simulation L4 of Table 2. Steady state is achieved after about 30 impeller revolutions.

As discussed before, power consumption is a crucial characteristic of stirred-tank reactors. In previous works,[24] power consumption was calculated from the total dissipation of power in the entire fluid volume. This calculation is representative of power consumption only under the hypothesis that the flow field reaches a steady state and that mean kinetic energy budget and turbulence kinetic energy budget do not change over time.[25,26] In the present work, we calculated the power

Table 2. Simulations Performed for Laboratory Reactor and Industrial Reactor

ref	density (kg/m^3)	viscosity (Pa·s)	rpm	*Re*	*Ne*
		laboratory reactor[a]			
L1	1259	0.825	200	165	0.952
L2	1181	0.025	80	2040	0.795
L3	1181	0.025	180	4592	0.748
L4	1000	0.001	80	43 200	0.709
L5	1000	0.001	200	108 000	0.702
		industrial reactor[b]			
R1	10	1	100	30	2.071
R2	1000	5	50	300	0.979
R3	1000	0.001	0.1	3000	0.896
R4	1000	1	100	3000	0.853
R5	1000	1.265	50	1 200 000	0.830
R6	1000	0.001	100	3 000 000	0.819

[a] For the laboratory reactor, the fluids and angular velocities are the same as for experiments. [b] For the industrial reactor, a broader range for Reynolds numbers is considered than for the laboratory reactor.

consumption, P, as the torque on the impeller blades and shaft times the angular velocity[11] using

$$P = \boldsymbol{\omega}\int_A \mathbf{r} \times (\boldsymbol{\tau}\cdot \mathrm{d}\mathbf{A}) \qquad (4)$$

where A is the overall impeller and shaft surface area, $\boldsymbol{\omega}$ is the angular velocity vector, $\mathbf{r}$ is the position vector, $\boldsymbol{\tau}$ is the stress tensor, and d$\mathbf{A}$ is the differential surface vector. The behavior of power consumption is shown in Figure 3c. From our observations, the main contribution to the torque is given by pressure rather than shear stresses. As discussed by Nagata,[7] the power develops over time through a peak and a slow decay toward the final steady state. Power consumption increases while the rotational flow extends out of the impeller region and gradually decreases as angular motion is established in the vessel. In some cases, and after 25 revolutions in our simulation, a decrease in power consumption is observed, which corresponds to transitions in the structure of the flow field.[7] Specifically, examining Figure 3b and c, we can see that, once the azimuthal component of the momentum is steady, the power consumption then decreases slightly. Broadly speaking, this effect depends on the decrease in the relative velocity between the impeller and the overall bulk of the fluid.

3.2. Comparison between Experiments and Simulations in the Laboratory Reactor. As seen in Table 2, we performed experiments in three different Reynolds number ranges: Reynolds order 100 (with glycerol), Reynolds order 1000 (with mixtures of water and glycerol), and Reynolds order 100 000 (with water). We decided to perform five computations for the laboratory reactor. This required an overall production time, not including the grid-sensitivity analysis or pre- and post-processing, of 30 days of CPU time on our server. Specifically, we simulated one set of operating conditions for the lower Reynolds number range and two sets of operating conditions for each experimental set in the range of higher Reynolds numbers, as shown in Table 2, where the corresponding power numbers are also reported.

For the sake of clarity, we plot the experimental measurements and numerical computations against the empirical curve calculated with the expression in the Appendix,[7] as shown in Figure 4. Figure 4 is on a bilogarithmic scale, and the experiments and computations accurately reproduce the expected Reynolds number−power number relation. In particular, the transition from laminar to turbulent behavior is captured in the Reynolds number range 10^2-10^3, and the power number becomes independent of the Reynolds number in the fully turbulent regime, $Re > 10^4$.

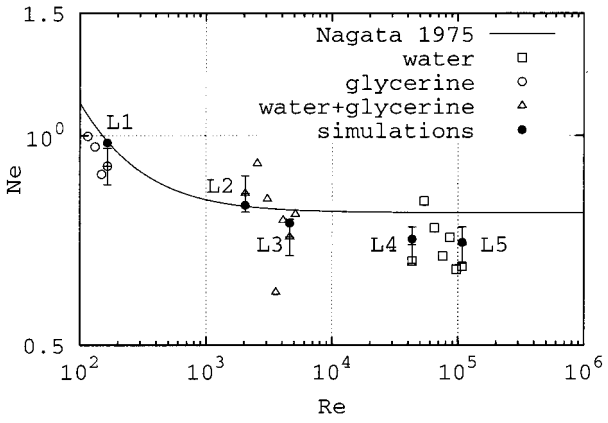

Figure 4. Fitting of experimental data and numerical data with empirical power characteristics by Nagata[7] (line). For experimental data, three ranges of Reynolds number are investigated using glycerol, water−glycerol solutions, and water. In each range, measurements are made for angular velocities in the range 80−200 rpm. Points calculated by numerical simulations (●) are within average experimental error (±6%) for the whole range of Reynolds numbers examined. Overall agreement with empirical correlation is good.

Experimental points corresponding to conditions simulated numerically are drawn with the error calculated in the turbulent range (6%), as discussed in the previous section. Given the characteristics of the experimental probe used to measure the power, the error bar calculated for the turbulent regime is likely to be an underestimation of the actual error affecting measurements in the laminar regime. The agreement between experiments and computations is good for all cases except for test L1, which is in the laminar regime.

3.3. Scale-up. *3.3.1. Industrial Measurements.* After the simulations had been run and analyzed, it was possible to measure the power dissipation on an industrial installation of the reactor for operating conditions corresponding to $Re = 2.4 \times 10^6$. The power number measured was $Ne = 0.760$ and was estimated from the power input to the impeller. Unfortunately, the working conditions of the industrial installation where the measurement was taken specified a volume of fluid in the tank equal to 10 000 L compared to the 12 500 L of our simulations. This corresponded to a height-to-tank diameter ratio $H/T = 1$ instead of 1.33 considered in our simulations that corresponds to the recommended filling of the tank.[27] From experiments, Armenante and Chang[8] observed that, if the liquid surface is high above the impeller, say, more than about one impeller diameter, power consumption is independent of the liquid height above the impeller. Other sources, such as the correlation by Nagata[7] reported in the Appendix, account for the H/T ratio explicitly. Thus, if we apply eq 14 in the Appendix to the industrial measurements, we can scale the measured Ne value up to $Ne = 0.866$.

3.3.2. Power Number−Reynolds Number Characteristics. The laboratory reactor and the industrial-size reactor are geometrically similar, as shown in Table 1. This similarity should ensure perfect scale-up.[28] We performed six simulations of the flow field in the industrial-size reactor, spanning a range of Reynolds

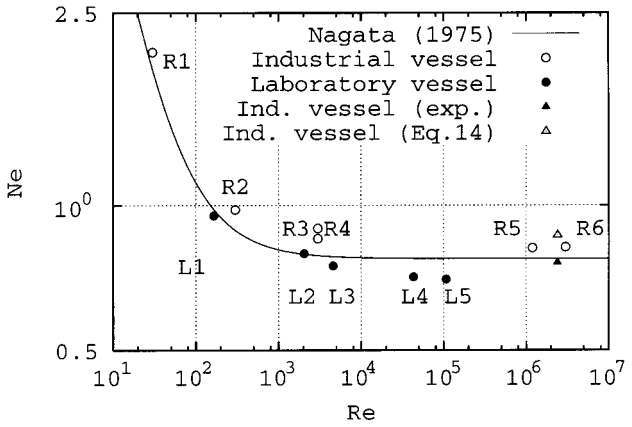

Figure 5. Comparison of empirical power characteristic curve from Nagata[7] (line) with computed results for the laboratory reactor (●) and the industrial vessel (○) and experimental data for the industrial reactor. In the fully turbulent range, simulations R5 and R6, empirical power characteristics, experimental data, and experimental data scaled for the H/T ratio can be compared.

numbers broader than that used for the laboratory reactor, as shown in Table 2. In Figure 5, we plot the power number values calculated for the industrial reactor, the values calculated for the laboratory-scale model, the measurements made on the industrial installation, the same measurements scaled by eq 14 of the Appendix, and the characteristic curve computed by applying the correlation by Nagata[7] to the industrial reactor.

Focusing on the fully turbulent region, we observe that the laboratory reactor shows power numbers lower than the industrial reactor. In a previous work, Bujalski et al.[29] observed a similar behavior and suggested a slight dependence of Ne on the tank size. In particular, provided that the impeller thickness-to-diameter ratio is kept constant, the power number should scale as

$$\frac{Ne_{\mathrm{ind}}}{Ne_{\mathrm{lab}}} = \left(\frac{T_{\mathrm{ind}}}{T_{\mathrm{lab}}}\right)^{0.065} \tag{5}$$

where suffixes indicate industrial and laboratory values. Even though this correlation was developed for reactors equipped with Rushton impellers,[29] in our case, it gives $Ne_{\mathrm{ind}} = 1.14Ne_{\mathrm{lab}}$. From our simulations, averaging the computed Ne values for the fully turbulent regime, we obtain $Ne_{\mathrm{ind}} = 1.168Ne_{\mathrm{lab}}$, in good agreement with the experimental observations of Bujalski et al.[29]

Turning now to the industrial measurements, we can examine the fully turbulent region in Figure 5, in which the measurements made on the industrial installation, the same measurements scaled by eq 14 of the Appendix, simulations R5 and R6, and the characteristic curve computed by applying the correlation by Nagata[7] to the industrial reactor are shown. The simulated asymptotic value for Ne is about 0.825—the average of R5 and R6—between the original value of the industrial measurement and its correction as scaled by eq 14. Observing further that the correlation by Nagata[7] predicts a value of 0.780 for Ne, we can consider our simulations to be accurate in the limit of the measurement error.

3.3.3. Pumping Capacity and Efficiency. The pumping capacity is the flow rate that crosses the impeller plane and is the crucial variable in evaluating the circulation in the reactor. For the reactor under investigation, the shape of the impeller and the clearance make it hard to define a section through which circulation can be easily evaluated. Because the impeller acts mainly as a radial impeller, we calculated the impeller flow by integrating the radial component of the velocity, v_r, on the minimal cylindrical surface coaxial with the impeller and enclosing the blades (at radial distance R_b) as follows

$$q_d = \int_{A_r} \mathbf{v}\cdot \mathrm{d}\mathbf{A}_r = \int_{z_b}^{z_t} 2\pi R_b v_r \, \mathrm{d}z \tag{6}$$

where $\mathbf{A}_r$ is the cylindrical surface with radial normal. The surface extends from the bottom of the tank, at height z_b, to the height of the blade tip, z_t. The flow ejected from the impeller, or the discharge flow q_d, is a submerged jet that expands to conserve its initial momentum. The interaction of the impeller jet and the surrounding fluid depends on the geometrical configuration of the vessel, i.e., impeller-to-tank diameter ratio, clearance of the impeller, and number of baffles, and establishes the upward flow, q_c, the evaluation of which is crucial for a number of mixing applications (e.g., solid suspension, homogeneization). We calculated the discharge flow for each set of operating conditions for the laboratory reactor and the industrial reactor. Then, to compare the values obtained on a common basis, we calculated the impeller flow number, N_{q_d}, as defined by Armenante and Chou,[24] by dividing the discharge flow by ND^3, i.e., the proportionality constant for the volumetric flow rate

$$N_{q_d} = \frac{q_d}{ND^3} \tag{7}$$

and we plotted the data obtained against the Reynolds number, as shown in Figure 6a. First, we notice that the values of N_{q_d} computed for the laboratory reactor and the industrial reactor can be fitted by a single line. Further, we observe that the discharge flow peaks in the Reynolds number range 2000−5000.

Finally, we evaluated the efficiencies of the two reactors. The efficiency is the flow generated per unit of power input and is defined[7] as

$$\eta = \frac{N_{q_d}}{Ne} \tag{8}$$

In Figure 6b, the values of efficiency are shown as a function of Reynolds number for all of the different operating conditions examined. The relationship between the efficiency and the Reynolds number is fundamental to evaluating the performance of the reactor under different operating conditions. From Figure 6b, it is apparent that the fluid dynamic performance of the laboratory replica can be scaled up to industrial size. Shifting attention now from the scale-up to the performances, we can observe from Figure 6b that, in the configuration examined, the fluid dynamic efficiency of the reactor has a peak for Re in the range of 10^3−10^4. This is caused by the high value of the discharge flow in the same range of Reynolds numbers.

4. Conclusions

The object of this work was to characterize quantitatively the fluid dynamics of an industrial-size CSTR. The reactor, equipped with a retreated curved-blade

Table 3. Correlation Parameters Obtained Using Empirical Equations 10−19 for CSTRs Examined

	A	B	p	C	Ne_∞	Ne_{max}	Ne_{max}/Ne_∞	Ne_B/Ne_∞	θ
laboratory vessel	32.94	1.003	1.508	1.138	0.228	1.138	4.983	2.94	90°
industrial CSTR	34.02	1.068	1.532	1.139	0.237	1.217	5.135	2.86	90°

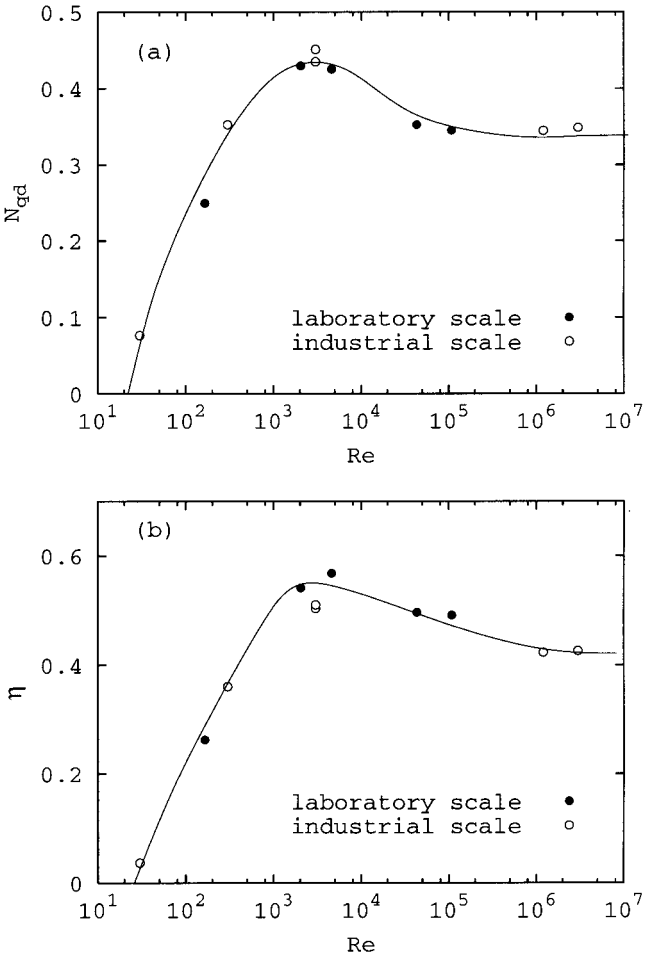

Figure 6. (a) Discharge flow number and (b) efficiency versus Reynolds number. Results computed for the laboratory vessel (●) and the industrial-size vessel (○) can be fitted by a single curve.

impeller and two beaver-tail baffles and lined with glass, has a nominal capacity of 12 500 L. This model is widely used for a number of applications, such as homogeneization, solid suspension, and crystallization. Because the large-scale size hampers direct measurements, we decided to exploit a small-scale (∼440:1 volume ratio) replica of the full-size reactor.

First, we performed experimental measurements of power consumption on the small-scale reactor, which we compared to fully three-dimensional time-dependent numerical simulations. We used the sliding-mesh approach to calculate the flow field in order to account for the impeller motion. The experiments and numerical simulations were in good agreement, within the range of experimental uncertainty.

Second, we performed numerical simulations of the flow field in the full-scale reactor for a broader range of Reynolds numbers. We were able to compare directly our simulations with one single measurement of the power input in a specific industrial installation and obtained satisfactory agreement. The empirical correlation developed by Nagata[7] also gave good results when compared to our simulations. From our simulations, we also detected a systematic dependence of the power number, Ne, on the tank size. A similar dependence was reported previously for reactors equipped with Rushton turbines.[29]

Finally, we were able to quantify the fluid dynamic efficiency of the reactor apparatus and define the Reynolds number range within which efficiency reaches an optimum value. We were also able to establish the validity of our computational procedures, obtaining good agreement with experiments and with the empirical curve.[7] Future developments include the evaluation of mixing in low-concentration dispersions. In this case, we will be able to consider the fluid dynamic fields calculated in this work to quantify and, hopefully, optimize the mixing of the CSTR.

Acknowledgment

Financial support from MURST under Grant 9809326392-005 and from Tycon-Technoglass is gratefully acknowledged. We thank in particular Ing. Lorenzo Sassetto and Mr. Gianni Artusi from Tycon-Technoglass for their useful and kind suggestions, as well as for making the small-scale apparatus available for experiments. Special thanks are also given to Ambra Ambroset, Alessandro Agosto, and Andreina Passon for performing some numerical simulations.

Appendix

Empirical Correlations. The general form of the power characteristic (see Nagata[7]) is

$$Ne = \frac{A}{Re} + B\left(\frac{10^3 + 0.6f\cdot Re^\alpha}{10^3 + 1.6f\cdot Re^\alpha}\right)^p \tag{9}$$

The first term represents the power consumption in the laminar range, and the second term represents the power consumption in the turbulent range. The coefficients of the empirical equation A, B, p, f, and α are estimated from the geometrical characteristics of the CSTR using the correlations experimentally derived from the data collected for a simple configuration (single-paddle impeller; $H/T = 1$; vertical blades, i.e., $\theta = 90°$)

$$A = 14 + \frac{b}{T}\left[670\left(\frac{D}{T} - 0.6\right)^2 + 85\right] \tag{10}$$

$$B = 10^{[1.3-4(b/T-0.5)^2-1.14D/T]} \tag{11}$$

$$p = 1.1 + 4\frac{b}{T} - 2.5\left(\frac{D}{T} - 0.5\right)^5 - 7\left(\frac{b}{T}\right)^4 \tag{12}$$

$$f = 2 \quad \alpha = 0.66 \tag{13}$$

Many corrections are needed for CSTRs having different configurations:

(1) To account for the effects of a different number of paddles and of a different type of impeller, an equivalent blade height, $b_{eq} = bn_p$, is used instead of b in eqs 10−13. The number of paddles, n_p, is calculated from the number of blades. Each blade is equivalent to 0.5 paddles.

(2) To account for the effect of liquid depth, a multiplicative factor C is used for the turbulent contribution to the power consumption

$$C = \left(\frac{H}{T}\right)^{0.35+b/T} \tag{14}$$

(3) To account for the effect of the blade inclination (θ), a multiplicative factor C_1 is used for the turbulent contribution to the power consumption

$$C_1 = (\sin\theta)^{1.2} \tag{15}$$

(3) To account for the effect of baffles, the geometrical characteristics of the baffles are used to determine the asymptotic value for the power dissipation. (a) For "fully baffled" conditions, this correction is given by

$$\left(\frac{B_w}{T}\right)^{1.2} n_B = 0.35 \tag{16}$$

corresponding to the maximum power consumption, Ne_{max}, given by

$$Ne_{max} = \frac{A}{Re} + BC \tag{17}$$

(b) For partially baffled conditions corresponding to a power number of Ne_B, the correction is given by

$$\frac{Ne_{max} - Ne_B}{Ne_{max} - Ne_\infty} = \left[1 - 2.9\left(\frac{B_w}{T}\right)^{1.2} n_B\right]^2 \tag{18}$$

where the power number obtained at Re tending to infinity, Ne_∞, is given by

$$Ne_\infty = B\left(\frac{0.6}{1.6}\right)^p \tag{19}$$

Correction factors are used to represent the following curves: (1) the "no-baffle" curve

$$Ne = \frac{A}{Re} + B\left(\frac{10^3 + 0.6f{\cdot}Re^\alpha}{10^3 + 1.6f{\cdot}Re^\alpha}\right)^p \tag{20}$$

(2) the "baffled" curve

$$Ne = \frac{A}{Re} + BCC_1\frac{Ne_B}{Ne_\infty}\left(\frac{10^3 + 0.6f{\cdot}Re^\alpha}{10^3 + 1.6f{\cdot}Re^\alpha}\right)^p \tag{21}$$

and (3) the "fully baffled" curve

$$Ne = \frac{A}{Re} + B\frac{Ne_{max}}{Ne_\infty}\left(\frac{10^3 + 0.6f{\cdot}Re^\alpha}{10^3 + 1.6f{\cdot}Re^\alpha}\right)^p \tag{22}$$

Dimensionless geometric parameters derived for the configurations examined are gathered in Table 1. These values are used to calculate the correlation parameters shown in Table 3, from which the functional representations of the power characteristics are obtained.

Literature Cited

(1) Nienow, A. W.; Hunt, G.; Buckland, B. C. A fluid dynamic study of the retrofitting of large agitated bioreactors: Turbulent flow. *Biotechnol. Bioeng.* **1994**, *44*, 1177.

(2) Jaworski, Z.; Nienow, A. W.; Koutsakos, E.; Dyster, K.; Bujalski, W. An LDA study of turbulent flow in a baffled vessel agitated by a pitched blade turbine. *Trans. Inst. Chem. Eng.* **1991**, *69*, 313.

(3) Ranade, V. V.; Joshi, J. B. Flow generated by pitched blade turbines. I: measurements using laser doppler anemometer. *Chem. Eng. Commun.* **1989**, *81*, 197.

(4) Kresta, S. M.; Wood, P. E. The mean flow field produced by a 45° pitched blade turbine: Changes in the circulation pattern due to off bottom clearance. *Can. J. Chem. Eng.* **1993**, *71*, 42.

(5) Zhou, G.; Kresta, S. M. Impact of tank geometry on the maximum turbulence energy dissipation rate for impellers. *AIChE J.* **1996**, *42*, 2476.

(6) Vrabel, P.; Van der Lans, R. G. J. M.; Luyben, K. C. A. M.; Boon, L.; Nienow, A. W. Mixing in large-scale vessels stirred with multiple radial or radial and axial up-pumping impellers: Modelling and measurements. *Chem. Eng. Sci.* **2000**, *55*, 5881.

(7) Nagata, S. *Mixing: Principles and Applications*; Kodansha: Tokyo, Japan, 1975.

(8) Armenante, P. M.; Chang, G. M. Power consumption in agitated vessels provided with multiple-disk turbines. *Ind. Eng. Chem. Res.* **1998**, *37*, 284.

(9) Brucato, A.; Ciofalo, M.; Grisafi, F.; Micale, G. Numerical prediction of flow fields in baffled stirred vessels: A comparison of alternative modelling approaches. *Chem. Eng. Sci.* **1998**, *53*, 3653.

(10) Sahu, A. K.; Kumar, P.; Joshi, J. B. Simulation of flow in stirred vessel with axial flow impeller: Zonal modeling and optimization of parameters. *Ind. Eng. Chem. Res.* **1998**, *37*, 2116.

(11) Harvey, A. D.; Rogers, S. E. Steady and unsteady computation of impeller stirred reactor. *AIChE J.* **1996**, *42*, 2701.

(12) Schafer, M.; Yianneskis, M.; Wachter, P.; Durst, F. Trailing vortices around a 45° pitched blade impeller. *AIChE J.* **1998**, *44*, 1233.

(13) Serra, A.; Campolo, M.; Soldati, A. Time-dependent finite-volume simulation of the turbulent flow in a free-surface CSTR. *Chem. Eng. Sci.* **2001**, *56*, 2715.

(14) Harvey, A. D.; Lee, C. K.; Rogers, S. E. Steady-state modeling and experimental measurement of a baffled impeller stirred tank. *AIChE J.* **1995**, *41*, 2177.

(15) Wechsler, K.; Breuer, M.; Durst, F. Steady and unsteady computations of turbulent flow induced by a 4/45° pitched-blade impeller. *J. Fluid Eng., ASME Trans.* **1999**, *121*, 318.

(16) Bartels, C.; Breuer, M.; Durst, F. Comparison between direct numerical simulation and $k-\epsilon$ prediction of the flow in a vessel stirred by a Rushton turbine. In *Proceedings of the 10th European Conference on Mixing*; van den Akker, H. E. A., Derksen, J. J., Eds.; Elsevier: Amsterdam, 2000; p 239.

(17) Ranade, V. V.; Joshi, J. B.; Marathe, A. G. Flow generated by pitched blade turbines. II: Simulation using $k-\epsilon$ model. *Chem. Eng. Commun.* **1989**, *81*, 225.

(18) Sahu, A. K.; Joshi, J. B. Simulation of flow in stirred vessel with axial flow impellers: Effects of various numerical schemes and turbulence model parameters. *Ind. Eng. Chem. Res.* **1995**, *34*, 626.

(19) Sahu, A. K.; Kumar, P.; Patwardhan, A. W.; Joshi, J. B. CFD modelling and mixing in stirred tanks. *Chem. Eng. Sci.* **1999**, *54*, 2285.

(20) Issa, R.; Ubbink, O. Numerical prediction of Taylor bubble dynamics using a new interface capturing technique. Presented at the3rd Joint Fluids Engineering Conference, San Francisco, CA, July 18−23, 1999; ASME Paper FEDSM99-7103.

(21) Campolo, M.; Agosto, A.; Ambroset, A.; Passon, A.; Paglianti, A.; Soldati, A. *Characterization of the Fluid Dynamics in Stirred Tank Reactors*; Technical Report CFI-RT 04-00; University of Udine, Udine, Italy, 2000.

(22) Montes, J. M.; Bolsom, H. C.; Fort, I.; Jahoda, M. Velocity field macro instabilities in axially agitated mixing vessel. *Chem. Eng.* **1997**, *67*, 139.

(23) Hasal, P.; Montes, J. M., Bolsom, H. C.; Fort, I. Macro instabilities of velocity field in stirred vessel: Detection and analysis. *Chem. Eng. Sci.* **2000**, *55*, 391.

(24) Armenante, P. M.; Chou, C. C. Velocity profiles in baffle vessel with single or double pitched blade turbines. *AIChE J.* **1996**, *42*, 42.

(25) Tennekes, H.; Lumley, J. L. *A First Course in Turbulence*; The MIT Press: Cambridge, MA, 1990.

(26) Soldati, A.; Banerjee, S. Turbulence modification by large-scale organized electrohydrodynamic flows. *Phys. Fluids* **1998**, *10*, 1742.

(27) Sassetto, L.; Artusi, G. Tycon-Technoglass. Personal comunication, S. Dona' di Piave, Italy, 2000.

(28) Sedov, L. I. *Similarity and Dimensional Methods in Mechanics*; Academic Press: New York, 1959 (translation by Morris Friedman from the 4th Russian ed.).

(29) Bujalski, W.; Nienow, A. W.; Chatwin, S.; Cooke, M. The dependency on scale and material thickness of power number of different impeller types. In *Proceedings of the International Conference on Mechanical Agitation*, ENS, Association of Chemical Engineers: Toulouse, France, 1986; Vol. 1, p 37.

(30) Campolo, M.; Soldati, A. Appraisal of fluid dynamic efficiency of retreated blade and turbofoil impellers in industrial size CSTR, submitted to *Ind. Eng. Chem. Res.*, 2001.

Received for review March 13, 2001
Revised manuscript received October 3, 2001
Accepted October 16, 2001

IE010225Y